Supporting Information for

A novel Colorimetric Method for Simultaneous Detection and Identification of Multi-Metal Ions in Water: Sensitivity, Selectivity and Recognition Mechanism

Linfeng Chen†, Xike Tian†,*, Dasha Xia‡, Yulun Nie†, Liqiang Lu†, Chao Yang† and Zhaoxin Zhou†

† Faculty of Materials Science and Chemistry, China University of Geosciences, Wuhan 430074, China

‡ School of Environmental and Chemical Engineering, Jiangsu University of Science and Technology, Zhenjiang 212003, China

Corresponding author: Xike Tian(xktian@cug.edu.cn)

Determination of association constant (Ka)

The association constant of the Tpy-QL and Tpy-BZ to metal ions were determined by the Benesi-Hildebrand analysis method. The UV-Vis spectra was recorded in 100% water solution in 10 mm cell and the absorption intensities of the probe meet the following formula:[1, 2]

$$\frac{1}{A - A_0} = \frac{1}{K_a(A_{max} - A_0)[M^{n+}]^x} + \frac{1}{A_{max} - A_0}$$

Where A_0 is the absorbance of free probe, A_{max} is the saturation absorbance of the Tpy-QL after adding metal ions, and A is the absorbance at different concentrations of metal ions (For Tpy-QL, absorbance intensity is obtained at 280 nm for Hg^{2+}, 520 nm for Co^{2+}, 607 nm for Fe^{2+}, and 598 nm for Fe^{3+}. For Tpy-BZ, absorbance intensity is obtained at 288 nm for Hg^{2+}, 520 nm for Co^{2+}, 637 nm for Fe^{2+}, and 630 nm for Fe^{3+}), K_a is the association constant, which is obtained by dividing the slope of the binding curve by the intercept.

Products characterization data

BZ: ^{1}H NMR (400 MHz, d_6-DMSO), δ (TMS, ppm): 8.48 (d, 1H), 8.36 (d, 1H), 7.92 (t, 1H), 7.83 (t, 1H), 4.80 (m, 2H), 3.32 (s, 3H) and 1.48 (t, 3H). HRMS (m/z) calcd for $C_{10}H_{12}NS$ $[M\text{-}I]^+$ 178.06788, found, 178.06891.

QL: ^{1}H NMR (400 MHz, d_6-DMSO), δ (TMS, ppm): 9.11 (d, 1H), 8.63 (d, 1H), 8.43 (d, 1H), 8.27 (d, 1H), 8.14 (d, 1H), 8.02 (d, 1H), 5.03 (m, 2H), 3.12 (s, 3H) and 1.56 (t, 3H). HRMS (m/z) calcd for $C_{12}H_{14}N$ $[M\text{-}I]^+$ 172.24688, found, 172.24639.

Tpy-BZ: ^{1}H NMR (400 MHz, d_6-DMSO), δ (TMS, ppm): 9.00 (s, 2H), 8.82 (d, 2H), 8.69 (d, 2H), 8.60 (m, 1H), 8.53 (d, 2H), 8.45 (m, 1H), 8.10 (m, 2H), 7.94 (m, 1H), 7.87 (m, 1H), 7.60 (m, 2H), 5.17 (m, 2H) and 1.55 (m, 3H). HRMS (m/z) calcd for $C_{26}H_{21}N_4S$ $[M\text{-}I]^+$ 421.14814, found, 421.14941.

Tpy-QL: ^{1}H NMR (400 MHz, d_6-DMSO), δ (TMS, ppm): 9.26 (d, 1H), 8.85 (s, 2H), 8.82 (t, 2H), 8.71 (t, 4H), 8.47 (d, 2H), 8.36 (d, 2H), 8.30 (m, 1H), 8.10 (m, 2H), 7.59 (m, 2H), 5.34 (m, 2H), 1.65 (t, 3H). HRMS (m/z) calcd for $C_{28}H_{23}N_4$ $[M\text{-}I]^+$ 415.19172, found, 415.19194.

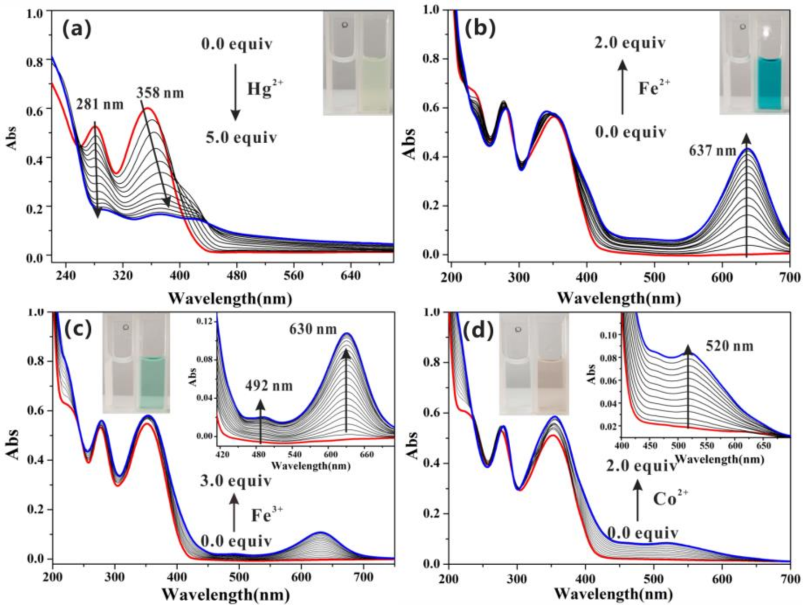

Figure S1. UV/Vis titrations spectra of Tpy-BZ (10 μM) in water at pH 7.0 in the presence of various concentration of (a) Hg^{2+} (b) Fe^{2+} (c) Fe^{3+} (d) Co^{2+}. The red line represents the spectrum of free Tpy-QL in water, blue line represents the spectrum after reaction saturation. The inset photographs were taken after the Tpy-BZ and metal ions were completely reacted.

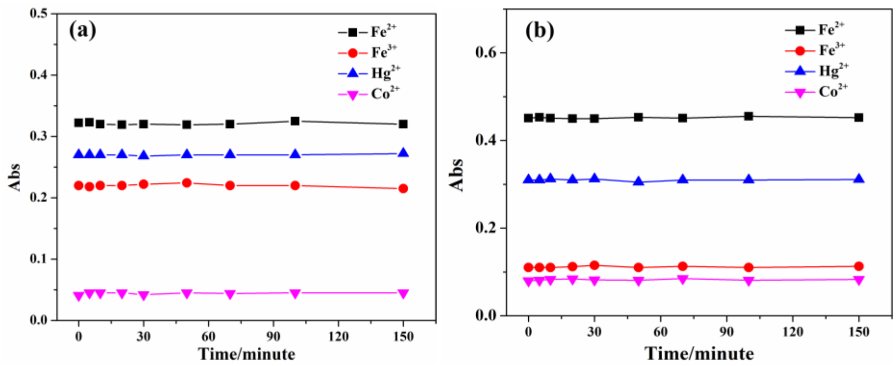

Figure S2. The stability of (a)Tpy-QL and (b)Tpy-BZ in aqueous solution after the addition of 3 equiv. of metal ions. (pH =7.0, Ex: 370 nm).

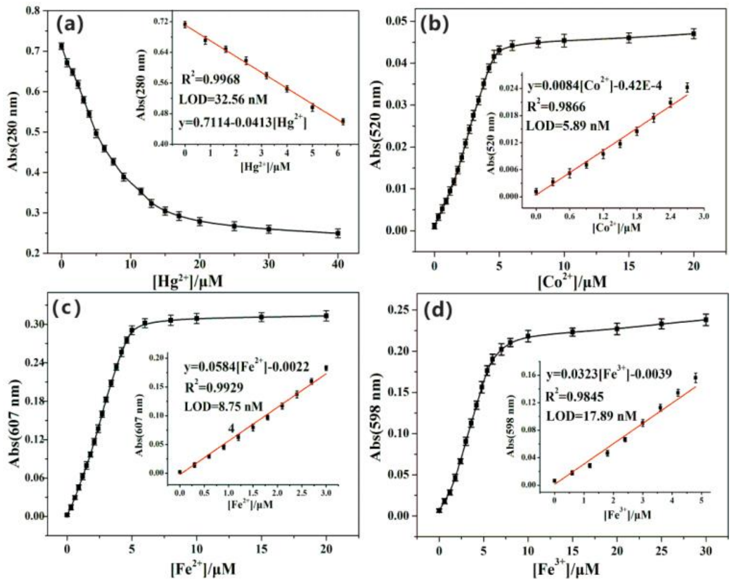

Figure S3. Absorbance intensity of Tpy-QL (10 μM) against the different concentrations of (a) Hg^{2+} (b) Co^{2+} (c)Fe^{2+} (d)Fe^{3+}. Inset: the linear relationship between absorbance intensity and (a) Hg^{2+} (b) Co^{2+} (c) Fe^{2+} (d) Fe^{3+} concentration.

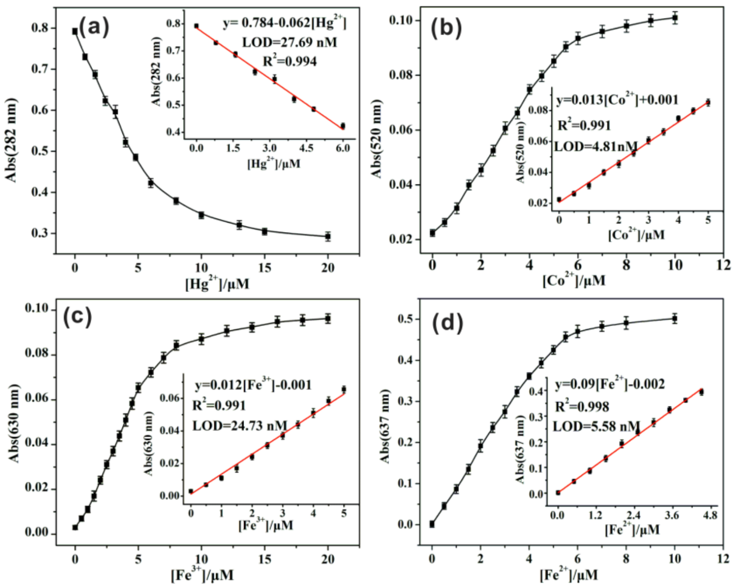

Figure S4. Absorbance intensity of Tpy-BZ (10 μM) against the different concentrations of (a) Hg^{2+} (b) Co^{2+} (c)Fe^{3+} (d)Fe^{2+}. Inset: the linear relationship between absorbance intensity and (a) Hg^{2+} (b) Co^{2+} (c)Fe^{3+} (d)Fe^{2+} concentration.

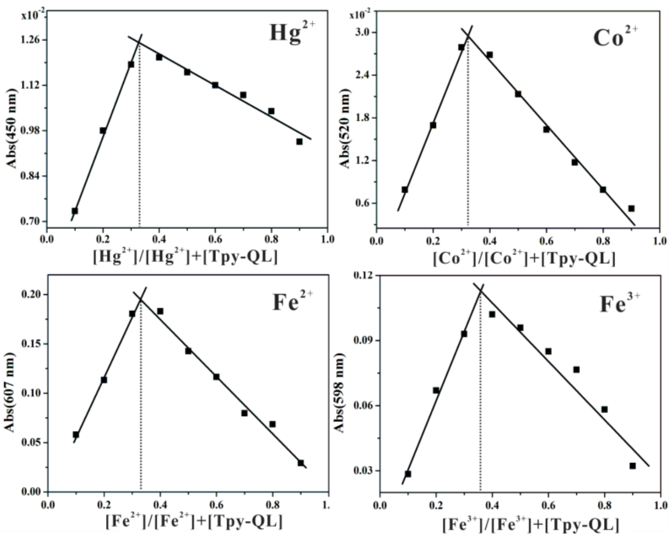

Figure S5. Job's plot of Tpy-QL with Hg^{2+}, Co^{2+}, Fe^{2+} and Fe^{3+} in 100% water solution (pH=7.0) (Total [Tpy-QL] + [metal ions] = 10 μM).

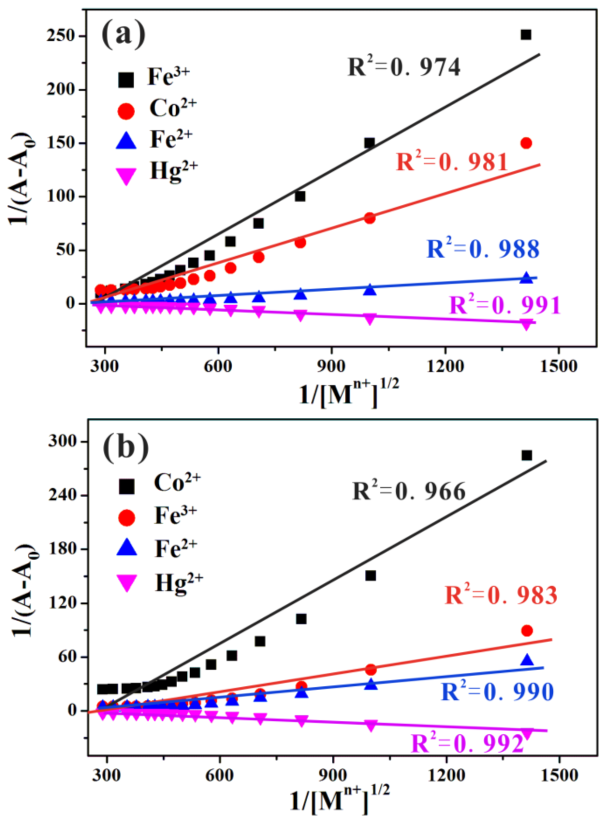

Figure S6. The Benesi-Hildebrand plot of (a) Tpy-QL and (b) Tpy-BZ with Hg^{2+}, Co^{2+}, Fe^{2+} and Fe^{3+}. A_0 is the absorbance intensity of free probe and A is the absorbance intensity at different concentrations of metal ions.

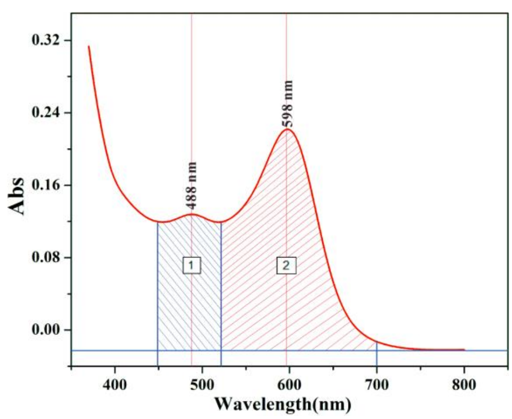

Figure S7. Calculation of the area of UV absorption peaks at 488 nm (S_{488}) and at 598 nm (S_{598}). The S_{488} is calculated from 450 nm to 520 nm, and the S_{598} is calculated from 520 nm to 700 nm.

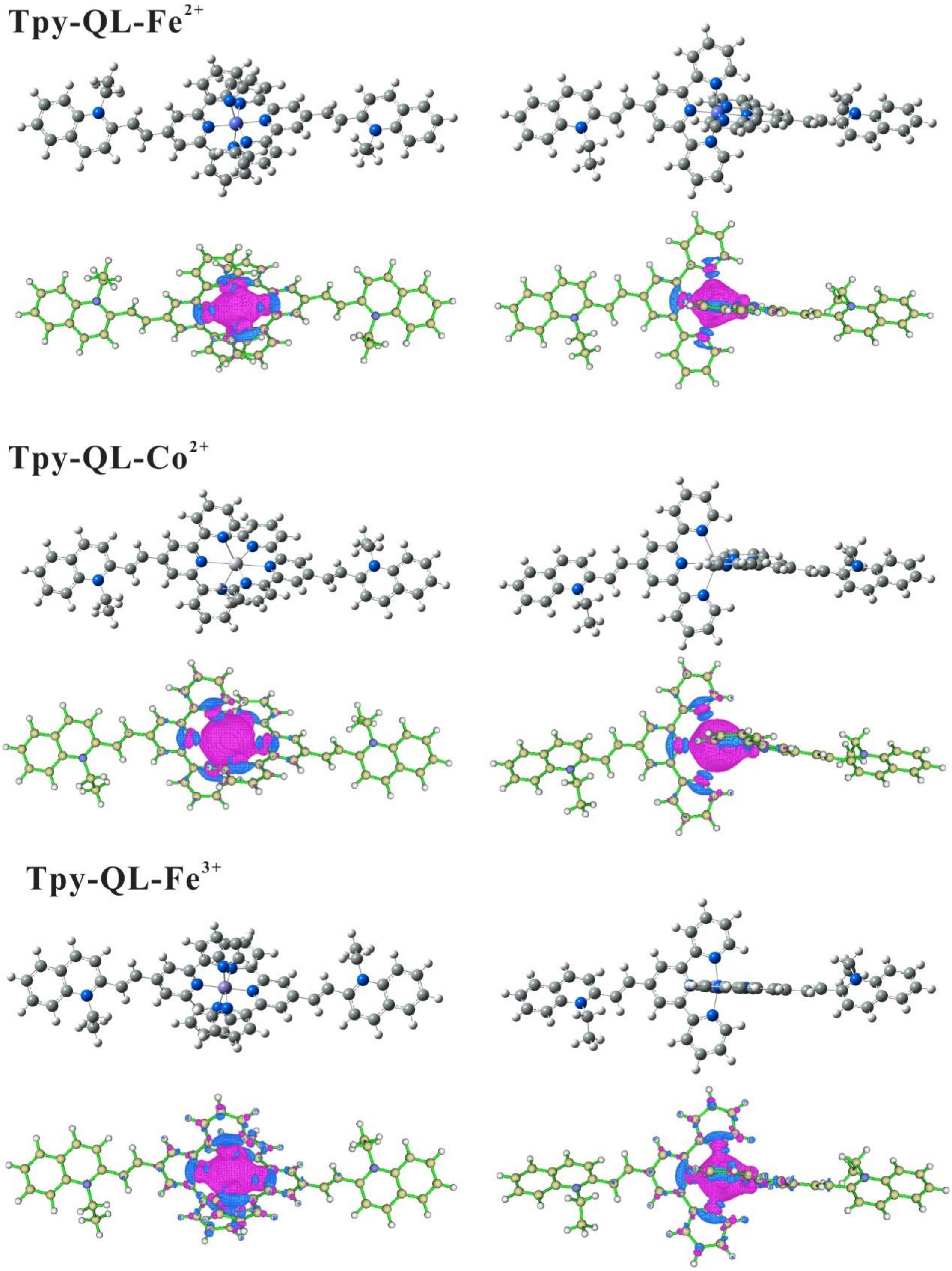

Figure S8. (up) Different observation view of DFT calculated optimization Tpy-QL-Fe^{2+} Tpy-QL-Co^{2+} and Tpy-QL-Fe^{3+} structure. (down) Corresponding electron density changes before and after the Tpy-QL reaction with metal ions. The color blue area indicates electron density decreases after the reaction, the purple area indicates electron density increase.

Table S1 Comparison of the detection limits for Co^{2+} colorimetric sensors

Colorimetric sensors for Co^{2+}	**Detection limit/ppb**
2-Aminothiophenol (ATP) and copper nitrate system[3]	2350
Ag nanoparticles[4]	0.58
Dithizone based colorimetric chemosensor[5]	2.32
Ag-Au bimetallic nanoparticles[6]	1.16
Sensitive ligand embedded nano-conjugate adsorbent[7]	0.19
Thiazole based ligands[8]	40
Chrysoidine G chemosensor[9]	100
Thiosulfate stabilized gold nanoparticles[10]	2.24
Tripodal amide ligand[11]	582
This work	**0.34**

Table S2 Comparison of the detection limits for Hg^{2+} colorimetric sensors

Colorimetric sensors for Hg^{2+}	**Detection limit/ppb**
Protein-functionalized gold nanoparticles.[12]	40
BSA-stabilized Pt nanozyme[13]	1.44
Chitosan-functionalized gold nanoparticles[14]	270
Label-free anisotropic nanogolds[15]	6
Hydrophilic cycloruthenated complex[16]	118
AIE-Based Chemodosimeter[17]	120
gold nanoparticles[18]	100
Colloidal Ag Nanocrystals[19]	40
Benzothiazole based colorimetric chemosensor[20]	102
Carbon nanodots as enzyme mimics[21]	4.6
Benzothiazole based colorimetric sensors[22]	80
Hg^{2+}-modulated G-quadruplex-based DNAzymes[23]	10
Silver nanoparticles [24]	3.4
This work	**6.51**

Table S3 Comparison of the detection limits for Fe^{2+} colorimetric sensors

Colorimetric sensors for Fe^{2+}	**Detection limit/ppb**
Electrospun nanofiber based colorimetric probe[25]	102
Dipicolylamine based sensor[26]	128
Hydrazinyl-4-(trifluoromethyl)pyrimidine[27]	21.1
Imidazole-based chemosensor[28]	17.9
8-Hydroxyjulolidine-9-carboxaldehyde[29]	64.4
Benzimidazole-based chemosensor[30]	66.1
2,3-Dihydroxybenzaldehyde[31]	30.8
TiO_2 based screen-printed material[32]	300
Schiff base based sensors based chemosensor [33]	7.84
Luminescent molybdenum disulfide nanosheet[34]	0.39
Sensor based on plasmonic response[35]	30.2
This work	**0.49**

Table S4 Comparison of the detection limits for Fe^{3+} colorimetric sensors

Colorimetric sensors for Fe^{3+}	**Detection limit/ppb**
Imidazole-based chemosensor[28]	15.1
8-Hydroxyjulolidine-9-carboxaldehyde based sensor[29]	28.6
Benzimidazole-based chemosensor[30]	67.8
Anionic poly(3,4-propylenedioxythiophene) derivative[36]	1.29
2,3-Dihydroxybenzaldehyde-based chemosensor [31]	14.0
1,8-Naphthalimide chemosensor[37]	384.2
Functionalized silver nanoparticles[38]	356.1
Naphthalenediimide based colorimetric probe[39]	5.6
Catalytic oxidation of gold nanoparticles[40]	47.6
Phenol-based BODIPY chemosensor[41]	7.84
Pyrophosphate functionalized gold nanoparticles.[42]	313.6
This work	**1.01**

Table S5 The structural parameters of coordination bond in the complex of Tpy-QL-M^{n+}

Complex	Bond angle of N-M-N(°)	Bond lengths of N-M (Å)	Angle of two Tpy-QL (°)
Tpy-QL-Hg^{2+}	81.55	1.97	91.28
Tpy-QL-Fe^{3+}	80.78	1.99	91.48
Tpy-QL-Fe^{2+}	79.89	1.92	91.76
Tpy-QL-Co^{2+}	73.88	2.07	94.71

[1]H NMR and HRMS data for obtained compounds

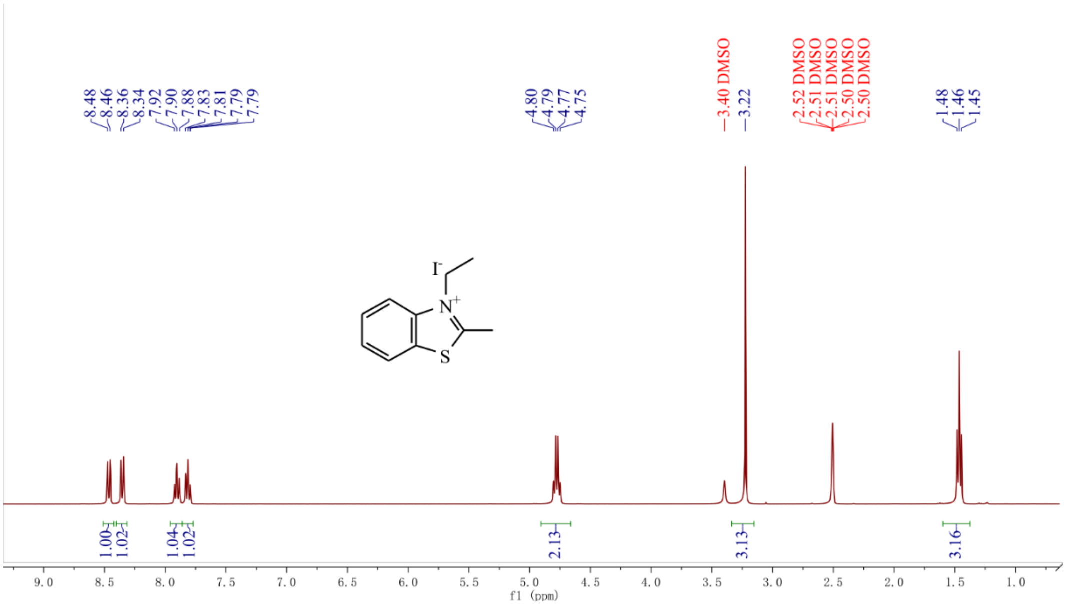

Figure S9. ^{1}H NMR of *N*-ethyl-2-methyl-benzothiazolium iodide in d_6-DMSO.

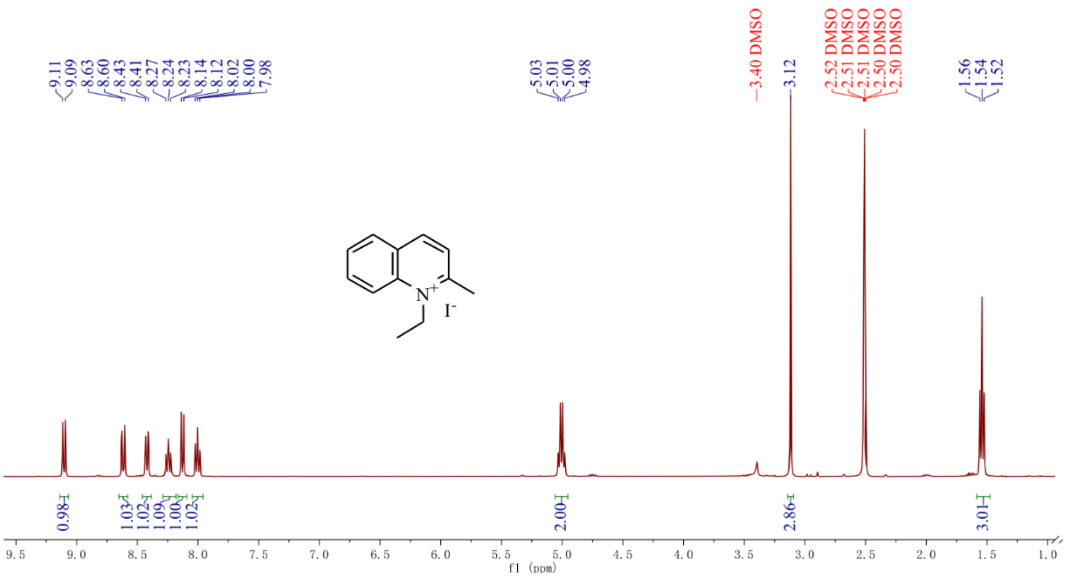

Figure S10. ^{1}H NMR of *N*-ethyl-2-methyl-quinolinium iodide in d_6-DMSO.

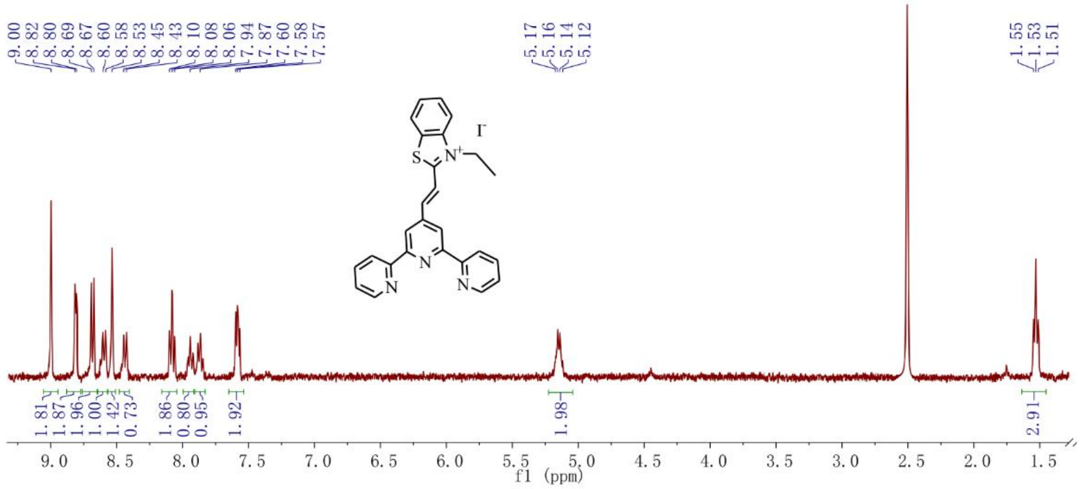

Figure S11. ^{1}H NMR of Tpy-BZ in d_6-DMSO.

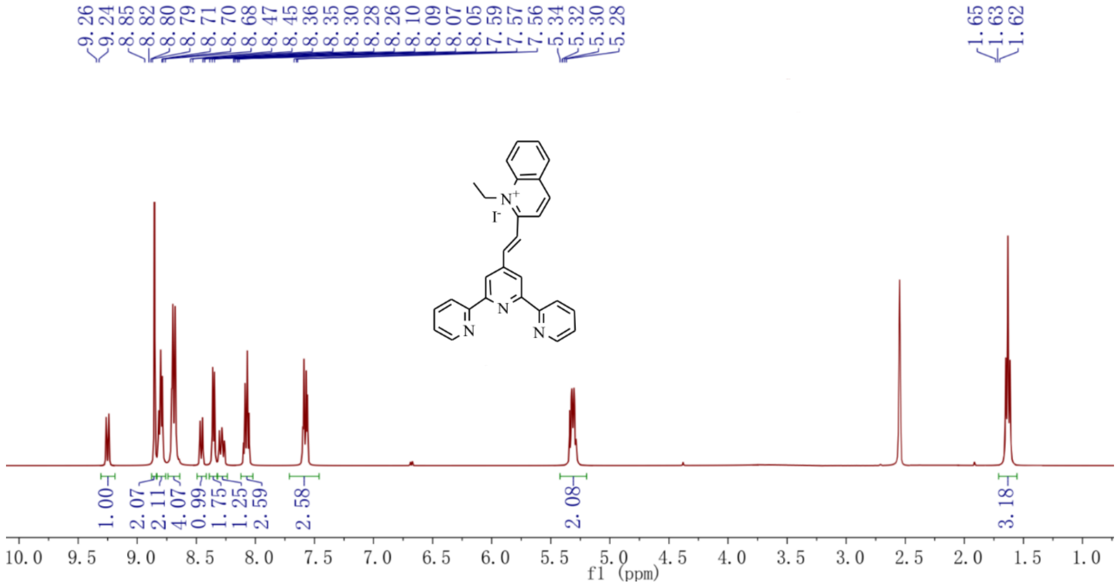

Figure S12. ^{1}H NMR of Tpy-QL in d_6-DMSO.

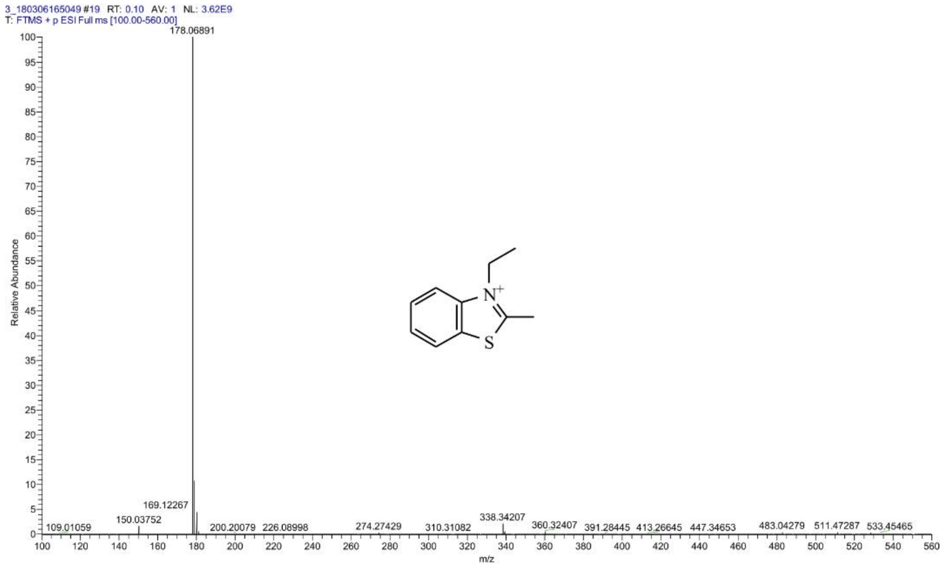

Figure S13. HRMS (m/z) analysis of the *N*-ethyl-2-methyl-benzothiazolium (calcd for $C_{10}H_{12}NS$ $[M-I]^+$ 178.06788, found, 178.06891).

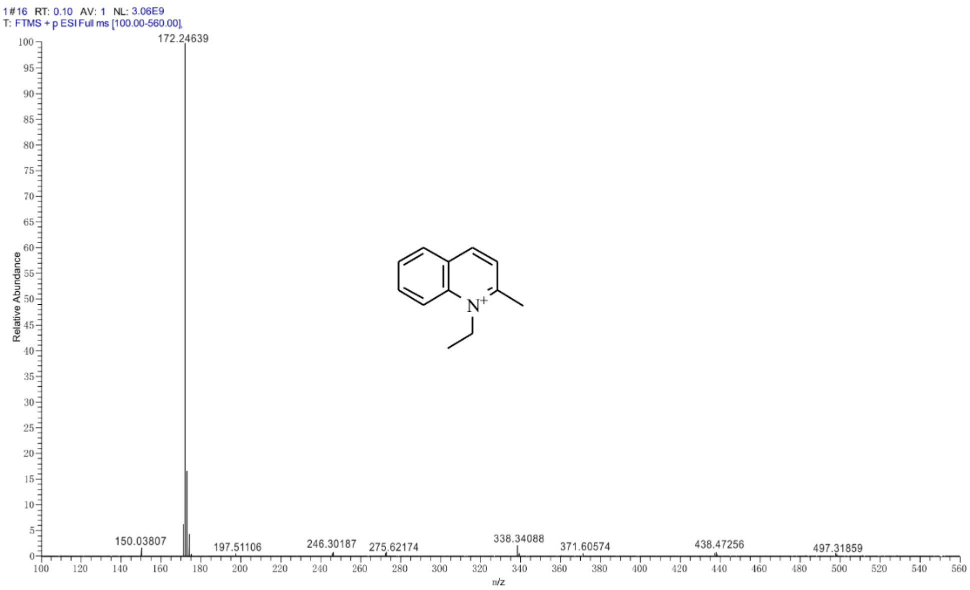

Figure S14. HRMS (m/z) analysis of the *N*-ethyl-2-methyl-quinolinium (calcd for $C_{12}H_{14}N$ $[M-I]^+$ 172.24688, found, 172.24639).

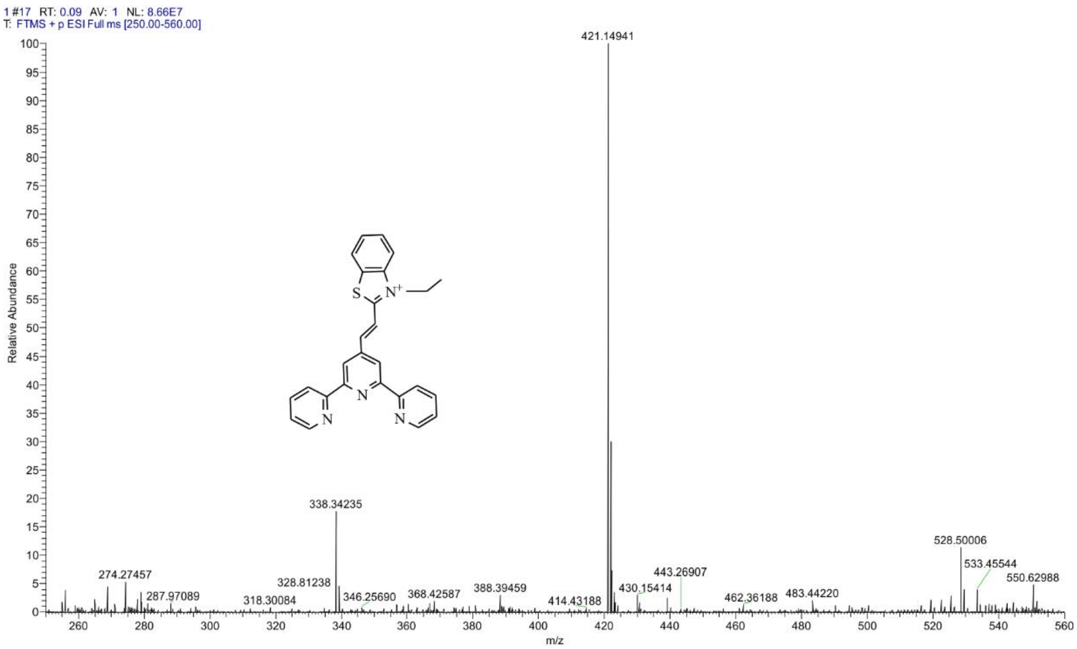

Figure S15. HRMS (m/z) analysis of Tpy-BZ (calcd for $C_{26}H_{21}N_4S$ $[M-I]^+$ 421.14814, found, 421.14941).

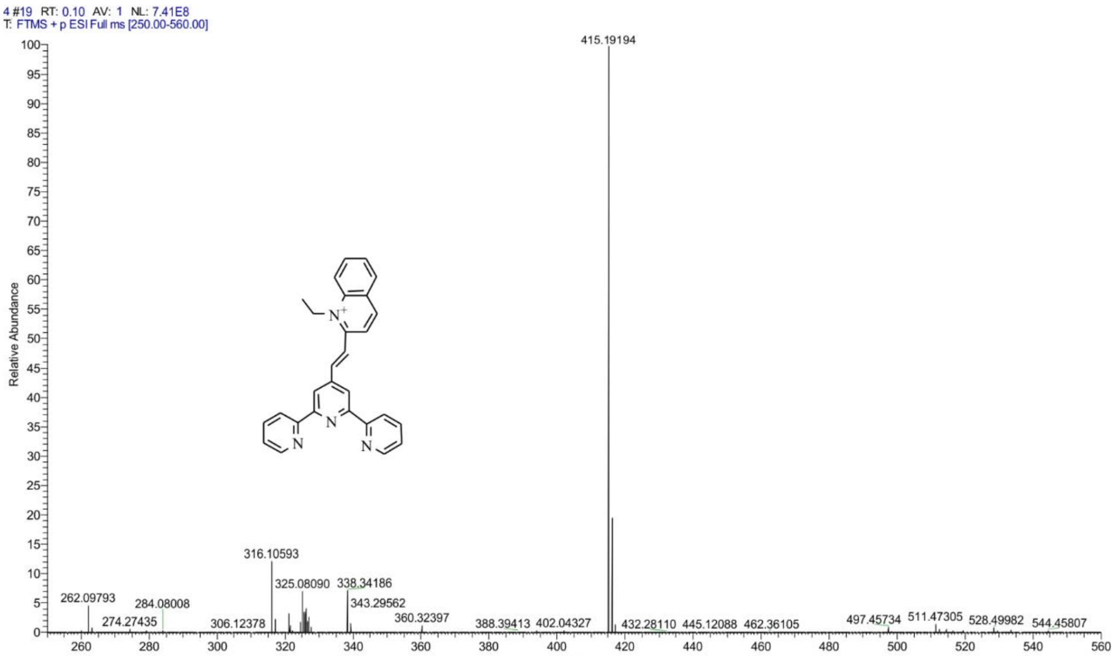

Figure S16. HRMS (m/z) analysis of the Tpy-QL (calcd for $C_{28}H_{23}N_4$ $[M-I]^+$ 415.19172, found, 415.19194).

References

1. I.D. Kuntz, F.P. Gasparro, M.D. Johnston, R.P. Taylor, Molecular interactions and the Benesi-Hildebrand Equation, *J. Am. Chem. Soc.* **1968**, *90,* 4778-4781.
2. H.A. Benesi, J.H. Hildebrand, A Spectrophotometric Investigation of the Interaction of Iodine with Aromatic Hydrocarbons, *J. Am. Chem. Soc.* **1949**, *71*, 2703-2707
3. Z. Liu, X. Jia, P. Bian, Z. Ma, A simple and novel system for colorimetric detection of cobalt ions, *Analyst* **2013**, *139,* 585-588.
4. T. Wu, Z. Ma, Colorimetric Detection of Cobalt or Nickel Ions Based on the Change of the Catalytic Performance of Leached Ag Nanoparticles, *J. Nanosci. Nanotechno.* **2017**, *17*, 4297-4303.
5. H. Tavallali, G. Deilamy-Rad, A. Parhami, S.Z. Mousavi, A novel development of dithizone as a dual-analyte colorimetric chemosensor: Detection and determination of cyanide and cobalt(II) ions in dimethyl sulfoxide/water media with biological applications, *J Photochem. Photobiol. B* **2013**, *125,* 121-130.
6. D. Xu, H. Chen, Q. Lin, Z. Li, T. Yang, Z. Yuan, Selective and sensitive colorimetric determination of cobalt ions using Ag-Au bimetallic nanoparticles, *RSC Adv.* **2017**, *7,* 16295-16301.
7. M.R. Awual, T. Yaita, H. Shiwaku, S. Suzuki, A sensitive ligand embedded nano-conjugate adsorbent for effective cobalt(II) ions capturing from contaminated water, *Chem. Eng. J.* **2015**, *276,* 1-10.
8. D. Singhal, A.K. Singh, A. Upadhyay, Highly selective potentiometric and colorimetric determinations of cobalt (II) ion using thiazole based ligands, *Mat. Sci. Eng. C-Mater.* **2014**, *45,* 216-224.
9. S.M. Kang, S.C. Jang, G.Y. Kim, C.S. Lee, S.H. Yun, C. Roh, A Rapid In Situ Colorimetric Assay for Cobalt Detection by the Naked Eye, *Sensors* **2016**, *16,* 626.
10. Z. Zhang, J. Zhang, T. Lou, D. Pan, L. Chen, C. Qu, Z. Chen, Label-free colorimetric sensing of cobalt(II) based on inducing aggregation of thiosulfate stabilized gold nanoparticles in the presence of ethylenediamine, *Analyst* **2011**, *137,* 400-405.
11. Z. JR, L. DP, H. Y, K. XJ, Z. ZM, R. YP, L. LS, H. RB, Z. LS, A highly selective colorimetric chemosensor for cobalt(II) ions based on a tripodal amide ligand, *Dalton T.* **2014**, *43,* 11579-11586.
12. Y. Guo, Z. Wang, W. Qu, H. Shao, X. Jiang, Colorimetric detection of mercury, lead and copper ions simultaneously using protein-functionalized gold nanoparticles, *Biosens. Bioelectron.* **2011**, *26,* 4064-4069.
13. W. Li, B. Chen, H. Zhang, Y. Sun, J. Wang, J. Zhang, Y. Fu, BSA-stabilized Pt nanozyme for peroxidase mimetics and its application on colorimetric detection of mercury(II) ions, *Biosens. Bioelectron.* **2015**, *66,* 251-258.
14. Z. Chen, C. Zhang, Y. Tan, T. Zhou, H. Ma, C. Wan, Y. Lin, K. Li, Chitosan-functionalized gold nanoparticles for colorimetric detection of mercury ions based on chelation-induced aggregation, *Microchim. Acta* **2015**, *182,* 611-616.
15. L.H. Jin, C.S. Han, Eco-friendly colorimetric detection of mercury(II) ions using label-free anisotropic nanogolds in ascorbic acid solution, *Sens. Actuators, B* **2014**, *195,* 239-245.
16. X. Li, X. Su, Z. Shi, X. Cheng, S. Liu, Q. Zhao, Highly selective and reversible colorimetric detection of mercury ions by a hydrophilic cycloruthenated complex in water, *Sens. Actuators, B* **2014**, *201,* 343-350.
17. A. Chatterjee, M. Banerjee, D.G. Khandare, R.U. Gawas, S.C. Mascarenhas, A. Ganguly, R. Gupta, H. Joshi, Aggregation-Induced Emission-Based Chemodosimeter Approach for Selective Sensing and Imaging of Hg(II) and Methylmercury Species, *Anal. Chem.* **2017**, *89,* 12698-12704.
18. N. Kanayama, T. Takarada, M. Maeda, Rapid naked-eye detection of mercury ions based on non-crosslinking aggregation of double-stranded DNA-carrying gold nanoparticles, *Chem. Commun.* **2011**, *47,* 2077-2079.

19. S. Liu, H. Yang, X. Zhao, Y. Ren, D. Li, L. Zhang, R. Xing, Microwave-Assisted Synthesis of Colloidal Ag Nanocrystals and Colorimetric Detection of Mercury (I and II) Ions in Aqueous Solution, *J. Nanosci. Nanotechno.* **2016**, *16,* 12326-12331.
20. B.K. Momidi, V. Tekuri, D.R. Trivedi, Selective detection of mercury ions using benzothiazole based colorimetric chemosensor, Inorganic *Chem. Commun.* **2016**, *74,* 1-5.
21. Z. Mohammadpour, A. Safavi, M. Shamsipur, A new label free colorimetric chemosensor for detection of mercury ion with tunable dynamic range using carbon nanodots as enzyme mimics, *Chem. Eng. J.* **2014**, *255,* 1-7.
22. A.K. Mahapatra, R. Maji, P. Sahoo, P.K. Nandi, S.K. Mukhopadhyay, A. Banik, A new colorimetric chemodosimeter for mercury ion via specific thioacetal deprotection in aqueous solution and living cells, *Tetrahedron Lett.* **2012**, *53,* 7031-7035.
23. T. Li, S. Dong, E. Wang, Label-free colorimetric detection of aqueous mercury ion Hg^{2+} using Hg^{2+}-modulated G-quadruplex-based DNAzymes, *Anal. Chem.* **2009**, *81,* 2144.
24. Y. Wang, F. Yang, X. Yang, Colorimetric detection of mercury(II) ion using unmodified silver nanoparticles and mercury-specific oligonucleotides, *ACS Appl. Mater. Inter.* **2010**, 2, 339.
25. D.A. Ondigo, Z.R. Tshentu, N. Torto, Electrospun nanofiber based colorimetric probe for rapid detection of Fe2+ in water, *Anal. Chim. Acta* **2013**, *804,* 228-234.
26. H. Kim, Y.J. Na, E.J. Song, K.B. Kim, J.M. Bae, C. Kim, A single colorimetric sensor for multiple target ions: the simultaneous detection of Fe^{2+} and Cu^{2+} in aqueous media, *RSC Adv.* **2014**, *4,* 22463-22469.
27. J.M. Jung, S.Y. Lee, C. Kim, A novel colorimetric chemosensor for multiple target metal ions Fe^{2+}, Co^{2+} and Cu^{2+} in a near-perfect aqueous solution: Experimental and theoretical studies, *Sens. Actuators, B* **2017**, *251,* 291-301.
28. T.G. Jo, K.H. Bok, J. Han, H.L. Mi, C. Kim, Colorimetric detection of Fe^{3+} and Fe^{2+} and sequential fluorescent detection of Al^{3+} and pyrophosphate by an imidazole-based chemosensor in a near-perfect aqueous solution, *Dyes Pigments* **2017**, *139*, 136-147.
29. H. Jung, H. Mi, highly selective colorimetric chemosensor for sequential detection of Fe^{3+} and pyrophosphate in aqueous solution, *Tetrahedron* **2017**, *73,* 6624-6631.
30. S.K. Yong, J.J. Lee, Y.L. Sun, T.G. Jo, C. Kim, A highly sensitive benzimidazole-based chemosensor for the colorimetric detection of Fe(II) and Fe(III) and the fluorometric detection of Zn(II) in aqueous media, *RSC Adv.* **2016**, *6,* 61505-61515
31. S.Y. Kim, S.Y. Lee, H.K. Ji, S.K. Min, A. Kim, C. Kim, Colorimetric detection of $Fe^{3+/2+}$ and fluorescent detection of Al^{3+} in aqueous media: applications and DFT calculations, *J. Coord. Chem*. **2018**, *6,* 1-21.
32. N.O. Laschuk, I.I. Ebralidze, S. Quaranta, S.T.W. Kerr, J.G. Egan, S. Gillis, F. Gaspari, A. Latini, O.V. Zenkina, Rational design of a material for rapid colorimetric Fe^{2+} detection, *Mater. Design*. **2016**, *107,* 18-25.
33. K.B. Kim, G.J. Park, H. Kim, E.J. Song, J.M. Bae, C. Kim, A novel colorimetric chemosensor for multiple target ions in aqueous solution: simultaneous detection of Mn(II) and Fe(II), *Inorg. Chem. Commun.* **2014**, *46,* 237-240.
34. Y. Wang, J. Hu, Q. Zhuang, Y. Ni, Enhancing sensitivity and selectivity in a label-free colorimetric sensor for detection of iron(II) ions with luminescent molybdenum disulfide nanosheet-based peroxidase mimetics, *Biosens. Bioelectron*. **2016**, *80,* 111-117.
35. S. Basiri, A. Mehdinia, A. Jabbari, A sensitive triple colorimetric sensor based on plasmonic response quenching of green synthesized silver nanoparticles for determination of Fe 2+ , hydrogen peroxide, and glucose, *Colloid.*

Surface. A **2018**, *545,* 138-146.

36. X. Chen, Q. Zhao, W. Zou, Q. Qu, F. Wang, A colorimetric Fe^{3+} sensor based on an anionic poly(3,4-propylenedioxythiophene) derivative, *Sens. Actuators, B* **2017**, *244,* 891-896.
37. Z. Zhang, S. Lu, C. Sha, D. Xu, A single thiourea-appended 1,8-naphthalimide chemosensor for three heavy metal ions: Fe^{3+}, Pb^{2+} and Hg^{2+}, *Sens. Actuators, B* **2015**, *208,* 258-266.
38. S. Bothra, J.N. Solanki, S.K. Sahoo, J.F. Callan, Anion-driven selective colorimetric detection of Hg^{2+} and Fe^{3+} using functionalized silver nanoparticles, *RSC Adv.* **2013**, *4,* 1341-1346.
39. N.V. Ghule, R.S. Bhosale, A.L. Puyad, S.V. Bhosale, S.V. Bhosale, Naphthalenediimide amphiphile based colorimetric probe for recognition of Cu^{2+} and Fe^{3+} ions, *Sens. Actuators, B* **2016**, *227,* 17-23.
40. J. Li, X. Wang, D. Huo, C. Hou, H. Fa, M. Yang, L. Zhang, Colorimetric measurement of Fe^{3+} using a functional paper-based sensor based on catalytic oxidation of gold nanoparticles, *Sens. Actuators, B* **2017**, *242,* 1265-1271.
41. L. Wang, G. Fang, D. Cao, A novel phenol-based BODIPY chemosensor for selective detection Fe^{3+} with colorimetric and fluorometric dual-mode, *Sens. Actuators, B* **2015**, *207,* 849-857.
42. S. Wu, Y. Chen, Y. Sung, Colorimetric detection of Fe^{3+} ions using pyrophosphate functionalized gold nanoparticles, *Analyst* **2011**, *136*, 1887-1891.